Review

Zhongming Huang, Xiao Cui, Shengliang Li*, Jinchao Wei, Peng Li, Yitao Wang* and Chun-Sing Lee*

Two-dimensional MXene-based materials for photothermal therapy

https://doi.org/10.1515/nanoph-2019-0571
Received December 31, 2019; revised February 12, 2020; accepted February 21, 2020

Abstract: MXenes, a new family of two-dimensional materials, are also known as transition metal carbides and nitride, with a general formula of $M_{n+1}X_nT_x$ ($n=1-3$). Their inherent metallic conductivity and hydrophilic nature endow MXenes with fascinating physicochemical properties (optical, electronic, magnetic, light-to-heat conversion. etc.). The ultrathin layer structure and photothermal property attract many interests in biomedical applications, especially as phototherapeutic agents for cancer treatment. In this review, we summarize the recent progress of MXenes in the field of photothermal therapy and highlight the crucial biotic index for their preparation and evaluation. First, we introduce the main strategies for the preparation and surface modifications of biologically applied MXenes. Then, representative cases in the field of MXene-based photothermal application, such as photothermal therapy, synergistic therapy, and targeting treatments, are reviewed. Finally, the cytotoxicity and *in vivo* long-term biosafety are introduced. We also propose the underlying challenges and perspectives for MXene applications in terms of photothermal therapy.

Keywords: MXenes; two-dimensional materials; photothermal therapy; synergistic therapy.

***Corresponding authors: Shengliang Li and Chun-Sing Lee,** Center of Super-Diamond and Advanced Films (COSDAF) and Department of Chemistry, City University of Hong Kong, Hong Kong SAR 999077, China, e-mail: lishengliang@iccas.ac.cn (S. Li); apcslee@cityu.edu.hk (C.-S. Lee). https://orcid.org/0000-0002-3890-8482 (S. Li); and **Yitao Wang,** Institute of Chinese Medical Sciences, State Key Laboratory of Quality Research in Chinese Medicine, University of Macau, Macau, China, e-mail: ytwang@um.edu.mo
Zhongming Huang and Xiao Cui: Center of Super-Diamond and Advanced Films (COSDAF) and Department of Chemistry, City University of Hong Kong, Hong Kong SAR 999077, China
Jinchao Wei: Institute of Chinese Medical Sciences, State Key Laboratory of Quality Research in Chinese Medicine, University of Macau, Macau, China; and Institute of Traditional Chinese Medicine and Natural Products, College of Pharmacy/Guangdong Province Key Laboratory of Pharmacodynamic Constituents of TCM and New Drugs Research, Jinan University, Guangzhou, China
Peng Li: Institute of Chinese Medical Sciences, State Key Laboratory of Quality Research in Chinese Medicine, University of Macau, Macau, China

1 Introduction

Emerging as a kind of novel two-dimensional (2D) material in 2011, MXenes are characterized by a few layered arrays of early transition metal atoms that are connected by a carbon or nitrogen atom layer between the metallic layers, also called transition metal carbides, and either nitrides or carbonitrides [1]. MXenes share a similar chemical formula, $M_{n+1}X_n$ ($n=1-3$), in which M stands for transition metal carbides (like Ti, Nb, Zr, Ta, Hf, V, Sc, Cr, Mo), and X is carbon or nitrogen [2]. Typically, MXenes show a lateral dimension range from nanometers to micrometers, while the thickness can reach nanometer levels [3]. More than 100 types of MXenes have been explored by computational methods; however, only >30 types have been achieved (Figure 1) [2]. In addition, the surface of MXenes is occupied by abundant hydrophilic groups such as fluorine (F), hydroxyl (OH), and oxygen (O), which endow MXenes with highly hydrophilic properties [4]. With both metallic conductivity and hydrophilic property, MXenes have been demonstrated to have broad applications in energy storage, electrocatalysis, water purification, and biosensing [5–8]. Specifically, the hydrophilicity of MXenes provide potentials for abundant biocompatible molecular grafting on the MXene surface, which extend their biomedical applications [9]. Besides the surface modification, the addition of other multi-functional materials like magnetic MnO_x or Fe_3O_4 onto MXenes by surface chemistry engineering can further broaden their biomedical applications [10, 11]. Meanwhile, the planar structure provides a large surface area, which makes MXene nanosheets qualified as carriers for cargo delivery [12].

Researchers have also focused on the optical properties of MXenes, like light absorption, emission, or

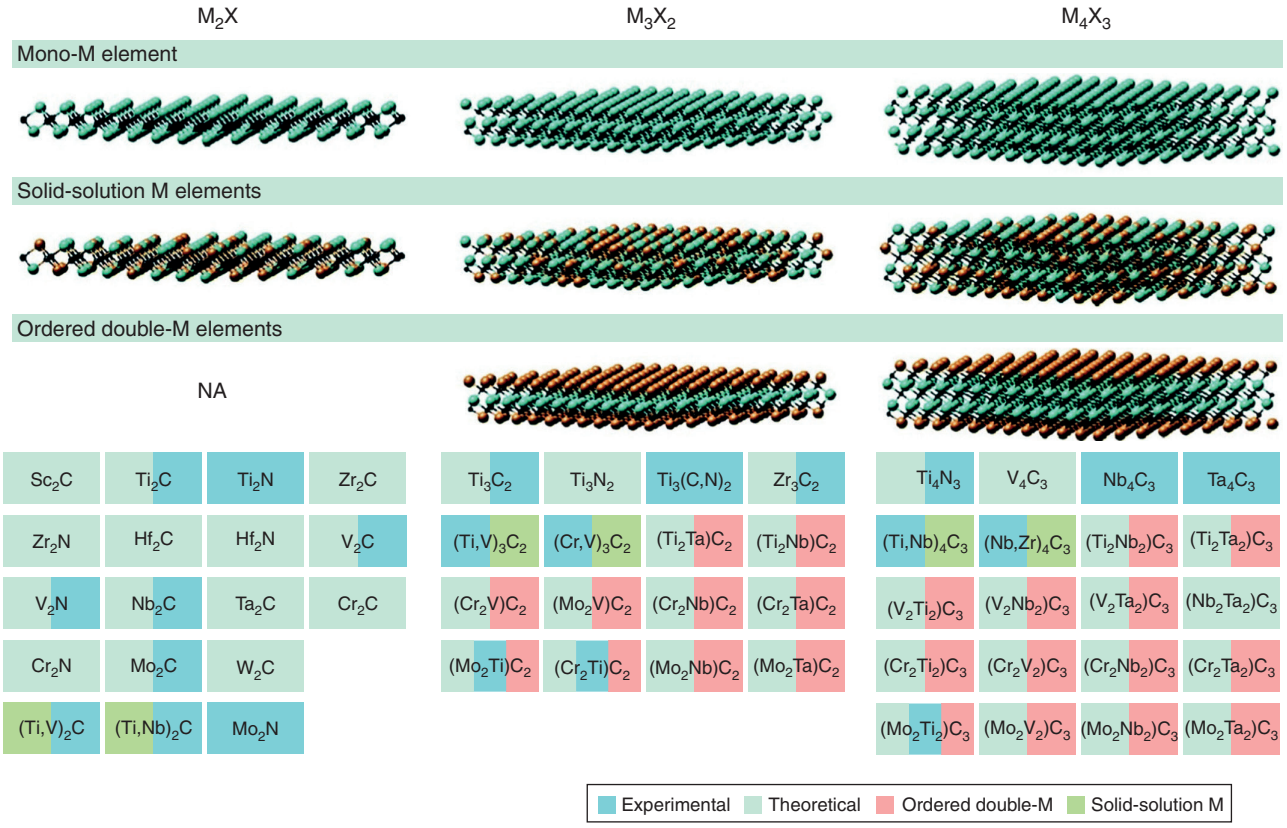

Figure 1: Recently reported MXenes mainly have three kinds of formulas: M_2X, M_3X_2, and M_4X_3, where M stands for early transition metal and X stands for carbon and/or nitrogen.
The first row shows the single-metal MXenes, for example Ti_2C, Ti_3C_2, Ta_4C_3, and Nb_4C_3. The second row shows the double-metal MXenes – solid solutes that contain two different metal elements, like $(Ti,V)_3C_2$ and $(Cr,V)_3C_2$. The third row shows the ordered double-transition metal MXenes in which one metal fills the outer M layers and another occupies the central layers (e.g. Mo_2TiC_2 and $Mo_2Ti_2C_3$, in which Mo fills the outer layer and Ti occupies the central layers).

scattering. Studies on the interactions between MXenes and light, including scattering, emission, and absorption, give insight to the interaction of 2D materials with photons, and provide promising candidates for widespread applications such as solar energy utilization, energy storage, catalysis, and bioimaging applications [13]. For the light emission property, similar with the well-developed 2D traditional luminescent materials like graphene quantum dots (QDs), g-C_3N_4 QDs, and MoS_2 QDs, luminescent MXene QDs can be achieved with tunable wavelength, high photostability, and acceptable quantum yield, which is mainly attributed to the small size and quantum confinement effect [14, 15]. The strong light-harvesting property of MXenes is highly favorable for light-to-heat conversion applications. The photothermal property of MXenes has been well studied in the field of photothermal therapy (PTT) for tumor ablation accompanied by photoacoustic imaging (PAI)-guided diagnosis. More encouragingly, desirable absorption ranges at the second biological window (biowindow) have been realized in MXenes, suggesting higher tissue penetration depth and larger maximum permissible exposure [16]. To date, various attractive MXene-based synergistic phototherapeutic agents that integrate chemotherapy/PTT/photodynamic therapy (PDT) together show great potential in PTT [17]. Other 2D nanomaterials like 2D monoelemental materials (Xenes) have attracted dramatically increasing attention owing to their excellent optical and electronic properties [18, 19]. The reported Xenes have demonstrated noteworthy advantages in the field of biosensors, bioimaging, therapeutic application, and theranostics [20–22]. For instance, the polyethylene glycol (PEG)-coated antimonene QDs from Xenes show a large extinction coefficient at near-infrared (NIR) absorption and remarkable photothermal performance that can be used for PTT for cancer [23]. Inorganic monoelemental 2D nanomaterials like graphdiyne have also been used as photothermal agents for simultaneous effective PAI and PTT for cancer [24].

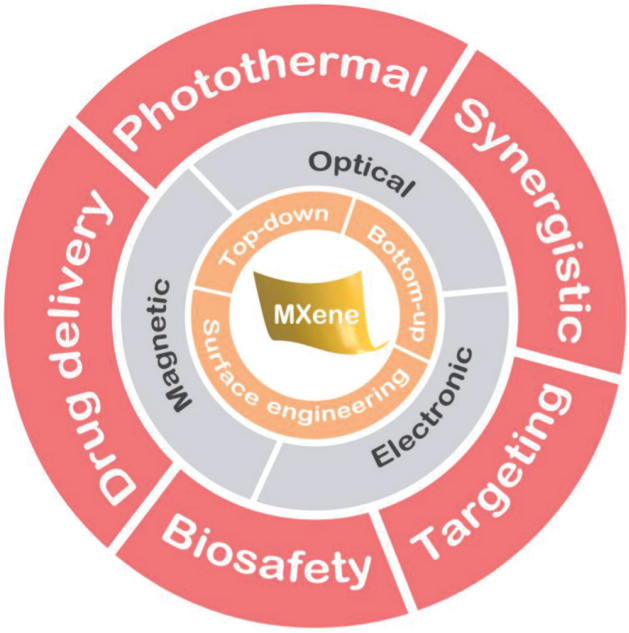

Scheme 1: Overview, properties, and advanced applications in the biomedical field of the developed 2D MXenes.

In this review, we highlight the advanced photothermal application of MXenes for cancer therapy. First, we systematically summarize the advanced development of preparation methods of MXenes and then discuss the surface engineering of these materials. Next, the unique properties of MXenes are introduced. Then, we emphasize the deeper insights on PTT for cancer as well as the biosafety in a living animal model (Scheme 1). Finally, we elaborate on the current challenges and future perspectives of MXenes for promising biomedical applications.

2 Synthesis of nanoscale MXenes

2.1 Top-down approach

Top-down fabrication methods primarily based on direct exfoliation transform relatively bulk layer-structure MXene ceramics into nanoscale by chemical etching [25]. As shown in Figure 2A, the underlying mechanism is the stronger chemical activity of the M-Al chemical bond than that of the M-C bond. Typically, transformation from bulk Ti_3C_2 MXene (Figure 2B, i) to multi-layer or nanoscale include the following two steps: First, MXene bulk precursors are treated with high-concentration HF, which is a powerful etching reagent selectively toward the middle Al layer (Figure 2B, ii) [26]. Then, the etched precursor is subjected to shearing forces or sonication under the assistance of delamination intercalants to obtain ultrathin or nanoscale products. Figure 2B (iii and iv) shows the transmission electron microscopy (TEM) and atomic force microscopy (AFM) images of Ti_3C_2 nanosheets. In terms of delamination intercalants, there are two types of intercalant: One is organic molecules like small organic molecules including dimethyl sulfoxide (DMSO) and N,N-dimethylformamide (DMF), or large organic base molecules including tetrabutylammonium hydroxide (TBAOH) and tetrapropylammonium hydroxide [27, 28], which can expand the interlayer spacing of MXenes and facilitate the etchant ions to reach the underneath unetched MAX precursors. The other type of intercalant is efficient for delamination of larger-size MXenes, which include inorganic materials such as halide salts or metal hydroxides [13].

In order to circumvent the use of harsh HF reagent in the exfoliation process, indirect HF etching methods are highly required and being developed. One proposed approach is *in situ* HF generation through the reaction between HCl and fluorides (LiF or NaF) [29]. Another alternative method is using molten fluorides at high temperatures [30]. Under high temperatures, free active F ions would corrode the attaching ions (Al, Si), thereby leading to an efficient etching. However, the involvement of F ions in the etching process indeed affects their future applications in biological environments because trace amounts of remaining F ions could be hazardous to organisms and induce cell death. In addition, this etching process primarily causes a fluorine-rich surface termination of MXene, which is a challenge for further surface modification before biological application.

Recently, fluorine ion-free etching has been proposed as an alternative approach for producing high-quality MXenes in nanoscale. Xuan et al. [31] use tetramethylammonium hydroxide (TMAOH) for delamination of bulk titanium carbide. This method fully utilizes the amphoteric nature of interlayer Al to form aluminum oxoanion functionalized titanium carbide, demonstrating intriguing optical absorption in the NIR region. Preliminary studies indicate that the prepared titanium carbide sheets can be used as efficient photothermal agents for killing tumor cells. Moreover, they show negligible cytotoxicity without light excitation even at high concentrations (50 μg ml^{-1}). Moreover, this method can also be used for producing ultrasmall sheets by simultaneous intralayer cutting and interlayer delamination upon powerful ultrasonication. The obtained ultrathin nanosheet structure was 2–5 nm in lateral width and with a thickness ranging from 0.5 to 1.5 nm. Yang et al. [32] demonstrated an efficient

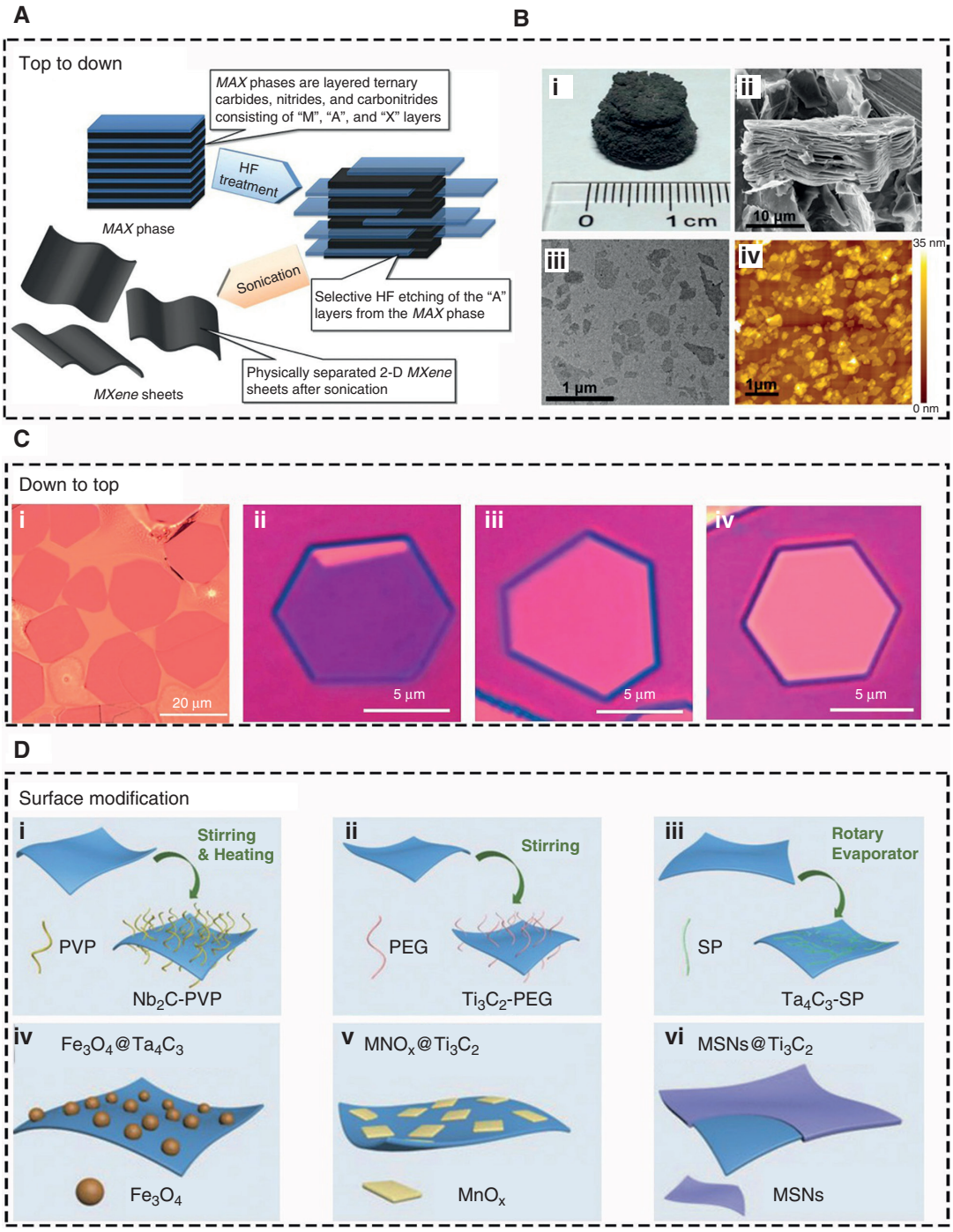

Figure 2: MXene preparation and surface modification methods.
(A) Schematic illustration of the top-down approach for MXene nanosheet preparation. (B) i, bulk Ti_3AlC_2 ceramic; ii, TEM of Ti_3C_2 after HF etching; iii, TEM of ultrathin Ti_3C_2 nanosheets after exfoliation; iv, AFM image of ultrathin Ti_3C_2 nanosheets after exfoliation. (C) i, optical image of Mo_2C crystal prepared by the bottom-up method; ii–iv, optical images of ultrathin Mo_2C crystal on a thick SiO_2/Si substance with 6.7, 8.2, and 11.2 nm, respectively. (D) Schematic illustration of MXene surface modification: i–iii, Nb_2C, Ti_3C_2, and Ta_4C_3 nanosheet surface modified with PVP, PEG, and SP, respectively; iv–vi, Ta_4C_3 and Ti_3C_2 nanosheet surface modified with Fe_3O_4 NP, MnO_x NP and MSNs, respectively.

fluoride-free etching fabrication method based on anodic corrosion of titanium aluminum carbide (Ti_3AlC_2) in binary aqueous electrolytes. After the dissolution of aluminum ions, extraction of carbide flakes was achieved by *in situ* intercalation of ammonium hydroxide into the flakes. The final products possess sizes ranging about 18.6 mm

and considerable high yield (>90%) of monolayers and bilayers. This safe strategy paves a way to obtain scalable products and to generally use MXene materials because the exfoliated $Ti_3C_2T_x$ (T = O, OH) flakes do not contain any fluorine terminations. Pang et al. [33] reported a novel thermal-assisted electrochemical etching method for facile and rapidly synthesized 2D MXenes. Additionally, those obtained 2D MXenes can be further used for multifunctional energy application, like oxygen evolution reaction and hydrogen evolution reaction.

2.2 Bottom-up approach

Compared with the top-down fabrication approach, bottom-up fabrication methods are more favorable for fabrication of 2D materials. By using the single inorganic atom or molecule as a precursor, well-tailed structures of MXenes are more easily formed through crystal growth. The intrinsic merit of the bottom-up approach is precisely controlling the parameters of MXenes, such as composition, size, morphology, or surface groups. Bottom-up methods are versatile for most traditional 2D materials such as graphene [34], g-C_3N_4 nanosheets [35], and MoS_2 nanosheets [36], mainly including chemical vapor deposition (CVD) growth or wet-chemistry synthesis. However, high-quality MXene fabrication by the CVD method is less reported. In 2015, fabrication of ultrathin α-Mo_2C crystals with large area and high quality through the CVD method was reported, and Figure 2C (i) shows the optical image of 2D ultrathin α-Mo_2C crystals [37]. By using methane as a carbon source and Cu/Mo foil as the metallic source, Mo_2C crystal was formed at a high temperature (>1085°C) with a large lateral size of >100 μm. Moreover, different thicknesses of Mo_2C crystal (6.7, 8.2, and 11.2 nm) can be obtained, and their corresponding optical images are listed in Figure 2C (ii–iv). As a paradigm, this work provided a facile and versatile strategy for the synthesis of transition metal carbides, which indicated the potential for the preparation of multi-component MXene crystals.

2.3 Surface engineering

Depending on the synthesis method, surface terminations mainly include hydroxyl (-OH), oxygen (-O), and fluorine (-F), which are bonded on the metal layers. Normally, the delaminated ultrathin MXenes are unstable in complex physiological conditions and lack multifunctionalization even though those surface terminations impart hydrophilic property to MXenes. Surface functionalization not only results in enhanced biocompatibility, circulation, targeting ability, and loading capacity but also avoids rapid aggregation and precipitation in biological media. Thus, surface engineering endows these nanosystems with high stability and dispersity in physiological environments and finally realizes various functionalities for effective biomedical application.

Recently developed surface modification methods are summarized in Figure 2D, which include molecular surface grafting and inorganic material surface engineering. The former modification type is mainly based on non-covalent interactions or electrostatic attraction for surface functional group change. For instance, polymer-based molecules, like polyvinyl pyrrolidone (PVP), PEG, and soybean phospholipid (SP) can be adsorbed on the surface of MXenes due to physical interaction [38–40]. The surface grafting processes are shown in Figure 2D (i–iii). Those molecules endow MXenes with excellent biocompatibility and stability. Among those developed modification methods, the SP-based strategy is commonly acknowledged as efficient and cost-effective. Besides the above-mentioned merits, MXenes with SP modification were also found to have long *in vivo* circulation and possess a good enhanced permeability and retention (EPR) ability in physiological environments [41]. Moreover, owing to the negative-charge surface terminals and large surface area, positively charged biomolecules such as doxorubicin (DOX) can be easily attached onto their surface by electrostatic attraction [42]. Furthermore, functional molecules that are negatively charged can be sequentially coated on the surface through a layer-by-layer strategy, in which the loaded drugs can be protected during the treatment or for precisely targeting drug delivery to the pathological site [i.e. arginine-glycine-aspartic acid (RGD) conjunction] [43]. Inorganic surface modification of MXenes integrates multi-functional inorganic nanoparticles onto the MXene, which could further broaden their potential applications (Figure 2D, iv to vi). For instance, MXene with magnetic nanoparticle (Fe_3O_4 NP) decoration can provide a typical magnetic resonance imaging (MRI) contrast agent with both therapeutic performance and diagnostic imaging function [11, 41]. Meanwhile, mesoporous silica nanoparticles (MSNs) decorating MXenes have been demonstrated as efficient drug delivery systems that show considerable drug delivery and releasing ability [43]. In summary, apart from those achievements, surface modifications on MXenes still need to be extensively explored in order to provide diverse multi-functional nanoplatforms for biomedical applications.

3 Properties of MXenes

3.1 Optical performances

Theoretical studies have shown that when materials interact with photons, photons can be absorbed as the materials' band gap corresponds to the photon's energy. For instance, depending on its metallic element composition, MXenes like Ti_2C, Zr_2C, and Hf_2C possess band gaps from 0.92 to 1.75 eV, which match well with photon energy in the visible light range [44, 45]. Additionally, by altering its surface groups, the band gaps can be tuned to match ultraviolet (UV) light. For example, researches have shown spectroscopic evidence that surface-functionalized sites in Ti_3C_2 MXene have a prominent effect on the light absorption property in the UV range. Besides light absorption in the UV and visible region, some MXenes also exhibit strong optical absorption with a wide range of spectra in the NIR region (>750 nm) (Figure 3A, B). Recent researches indicated that few MXenes such as Nb_2C exhibit strong optical absorption in the second biowindow (NIR-II, 1000–1350 nm; Figure 3C), which endows them with high photothermal conversion efficiency (PCE; up to 50%) for deep-tissue PTT and PAI [10, 38].

MXenes have been evidenced as promising substrates for Raman scattering signal enhancement owing to their intriguing physiochemical characteristics, such as highly metallic conductivity and flexible surface (Figure 3D). This enhancement effect is attributed to the intensive localized surface plasmon resonance effect, and its flexible and large surface area can provide a close and stable interaction with the Raman tags [46]. Taking advantage of MXenes as surface-enhanced Raman scattering (SERS) substrates, Raman scattering-based sensors or high-resolution Raman imaging can be

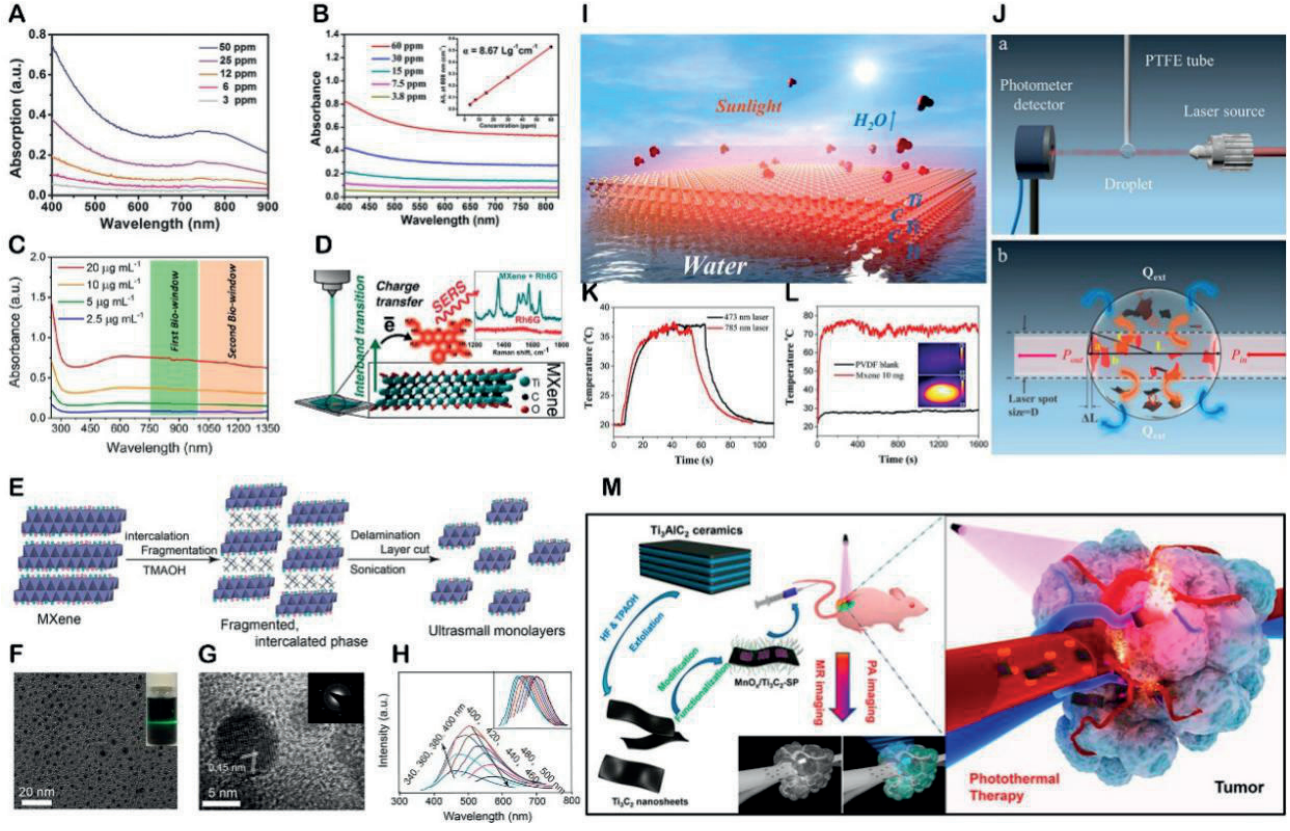

Figure 3: Properties of various MXene nanosheets.
(A) Absorbance spectra of Ti_3C_2 MXene nanosheets at varied concentrations. (B) Light absorption ability of Ta_4C_3 nanosheets dispersed in water. (C) Light absorption ability of Nb_2C MXene nanosheets at both NIR-I and NIR-II biowindows. (D) MXenes serving as the substrate for light-scattering application. (E) Synthesis method for producing fluorescent ultrasmall Ti_3C_2 MXene dots. (F, G) TEM and high-resolution TEM image of Ti_3C_2 MXene dots. (H) Excitation-dependent emission phenomenon of the MXene dots. (I) Schematic illustration of light-to-heat conversion of Ti_3C_2 MXene nanosheets. (J, K) Experimental setup for light-to-heat conversion meas urement and temperature initialization after laser off. (L) Temperature profiles of MXene-PVDF membrane under 1 sun irradiation. (M) Schematic illustration of Ti_3C_2 MXene nanosheets for PTT application.

achieved *in vitro* and *vivo*, which provide an attractive substitute for biosensor development and bioimaging-guided therapeutic applications [47].

Generally, bulk MXene, exfoliated multi-layer MXene, and single-layer MXene nanosheets are non-emissive. The recently reported small-sized MXene QDs are emissive and have been demonstrated as promising luminescent materials for bioimaging. Owing to the size-effect-induced quantum confinement and defect-induced luminescence, the reported MXene QDs show intriguing luminescent properties like tunable wavelength, high photostability, and desirable quantum yields (around 10%), which are suitable for bioimaging [14]. Up to now, the main MXene QD preparation method is the top-down cutting method, including the hydrothermal or solvothermal method (Figure 3E). TEM and high-resolution TEM images of prepared MXene QDs are shown in Figure 3F and G. Furthermore, the reported colloid MXene QDs showed excitation-dependent emission behavior, which is very similar to the property of hydrothermally synthesized carbon or graphene QDs. This phenomenon may be attributed to the optical selection of different sizes or surface defects on the QD surface. Corresponding fluorescence peaks red-shifted from 460 to 580 nm with increasing excitation wavelength from 340 to 500 nm (Figure 3H) [13].

3.2 Electronic properties

The electronic properties of MXenes mainly depend on the internal orderly arrayed metal atom. The conductive metallic nature endows MXenes with unusual conductive or semiconductor properties. This is attributed to the free electrons that could freely flow within the metallic outer layers. Although MXenes like Ti_2C, Ti_3C_2, Mo_2C, Mo_2C_2, and $Mo_2T_2C_3$ have been confirmed to have good electronic properties, conductive insulation can be found only in some heavy transition metals (e.g. Cr, Mo) containing MXenes [48]. Besides the achieved initial success, much efforts need to be devoted in studying the electronic property of MXenes as its importance is realized.

Another factor that influences the electronic property of MXenes is the preparation method. Diverse preparation methods lead to various surface terminations, and those terminal groups possess different abilities to attract electrons and significantly affect the conductivity of MXenes [49]. Through surface engineering by changing terminal groups, the modified MXenes can be employed as electrochemical sensors for several gases or specific molecules. The mechanism is attributed to the inevitable conductivity changes when the analytes are attached onto the surface of modified MXenes [50]. Apart from surface modification, surface defects can also be induced in the preparation process or by external element doping, which also significantly influences the conductivity. The increasing number of surface defects leads to restriction on the free movement of electrons as well as causes imbalance of electronic density within the metallic layer [51]. Another significant property of MXenes is that the active electrons and vacancies could be generated under certain external stimuli, such as heat or light. On the basis of this semiconducting property, MXenes could also be employed for reactive oxygen species (ROS) generation or catalyst-related applications [17]. For instance, the generated vacancies can react with substrates and subsequently impose oxidative stress on them. Additionally, by regulating the band gap by changing the surface terminations, inducing defects, or doping certain ions, MXenes can be responsive to various types of stimuli. These intriguing properties are essential for their applications, such as in biosensors, antimicrobial usage, and biomedicine.

The magnetic properties of MXenes are less reported compared with their conductivity and semi-conductivity properties. The investigation of magnetic properties is still in the theoretical study period. Recent theoretical studies indicated that two types of MXenes, chromium carbide (Cr_2C) and chromium nitride (Cr_2N), have been indicated to have magnetic properties without surface termination configuration [52]. However, the preparation of termination-free MXenes is not yet reported. Thus, further experimental confirmation for the magnetic properties is still demanded. Recently reported magnetic MXenes integrated inorganic magnetic nanomaterials like manganese oxide (MnO_x) and iron oxide (Fe_3O_4) formation as novel multi-functional materials [10, 11]. These kinds of hybrid magnetic materials have significantly broad biomedical applications, such as in MRI-guided diagnosis.

3.3 Photothermal conversion

Photothermal conversion is another important property of MXenes. With light-to-heat conversion, MXenes have been applied in thermal-catalytic reactions, solar energy utilization, water distillation, and PTT. However, the theoretical mechanism of MXene photothermal conversion is rarely studied. Recently reported MXene materials have been successfully applied in the solar energy technology (Figure 3I). The photothermal performance of Ti_3C_2 measured with a photometer detector under laser irradiation and heat generation process is illustrated in Figure 3J. The results confirmed that Ti_3C_2 can achieve almost 100% internal

light-to-heat conversion (Figure 3K). Stacked MXenes on a polyvinylidene fluoride (PVDF) film show efficient light-to-heat conversion (Figure 3L), and the evaporation efficiency for steam generation can reach up to 84% under 1 kW m^{-2} solar light irradiation. Those results demonstrate that MXenes are promising solar photothermal materials for seawater desalination, water purification, and other solar energy utilization technology [53]. Additionally, the photothermal property of MXenes is essentially favorable for PTT owing to the high PCE. For instance, recently reported biocompatible Ti_3C_2 nanosheets showed potential in the *in vitro/vivo* photothermal ablation of tumors by generating local heat at the pathological site under laser irradiation (Figure 3M) [54].

4 Photothermal applications

4.1 PTT

PTT for tumor eradication has drawn considerable research enthusiasm. There are two basic components that influence the PTT performance: external light and photothermal agents. Typically, photothermal agents are accumulated within tumors and generate local heat under light irradiation, and subsequently cause a hyperthermia effect to kill cancer cells [55]. PTT is a promising modality for tumor eradication with local hyperthermia while minimizing the adverse effects. For photothermal agents, two factors are considered as fundamental parameters that principally influence their corresponding PTT performance. One is the capability of light absorption, which is determined by the extinction coefficient (ε), and the other is the ability to generate heat under external light irradiation, which is also known as PCE (η). To improve the photothermal conversion performance, photothermal materials such as carbon-based materials, plasmonic metallic nanomaterials, inorganic multi-functional materials, and organic materials have been reported. Despite those achievements, the relatively small extinction coefficient and low PCE limit the broad application for advanced PTT. The recently emerging 2D MXenes have demonstrated significant PCE compared with the above-mentioned materials due to the strong absorption in the NIR range, indicating that MXenes can be used as efficient photothermal agents. Lin et al. reported 2D biocompatible Ti_3C_2 nanosheets by HF etching bulk MAX phase Ti_3AlC_2 with surface SP modification (Figure 4A) [56]. The obtained ultrathin Ti_3C_2-SP nanosheets possess monolayer or few-layer thickness with a remarkably high extinction coefficient (ε) of 25.2 l g^{-1} cm^{-1}, which is much higher than that of GO nanosheets (3.6 l g^{-1} cm^{-1}) or gold nanorods (13.9 l $g^{-1}cm^{-1}$). Figure 4B shows that the obtained Ti_2C_3-SP nanosheets have broad light absorption capability from 400 to 900 nm, indicating a favorable NIR laser-absorption property. Upon NIR laser irradiation for 6 min, the temperature of Ti_2C_3-SP nanosheet dispersion can quickly reach 55°C (Figure 4C), implying that the Ti_2C_3 nanosheets can rapidly convert NIR light into heat. *In vitro* photothermal performance was confirmed by live-dead cell staining, in which red fluorescence represents dead cells and green fluorescence represents live cells. The results indicated that the majority of 4T1 cells were ablated by hyperthermia after Ti_2C_3-SP nanosheet treatment. Moreover, *in vivo* photothermal ablation of tumors is also proved in xenograft tumors in a mouse model. Infrared thermal images and photographs of tumor-bearing mice are shown in Figure 4D and E. After 20 mg kg^{-1} Ti_3C_2-SP administration, Ti_3C_2-SP accumulated in the tumor site and exhibited a good photothermal conversion *in vivo*. Tumor volume changes were also recorded during the therapy process, and the results indicated that Ti_3C_2-SP nanosheets with laser irradiation show an effective tumor inhibition property (Figure 4F).

Although a considerable PCE can be achieved using Ti_3C_2-SP nanosheets as photothermal agents (30.6%), a recent study has revealed that Ta_4C_3-SP nanosheets possess superior PCE (44.7%) under 808-nm laser irradiation and have been utilized in PTT (Figure 5A) [57]. These biocompatible Ta_4C_3-SP nanosheets show a sheet-like morphology with a lateral size of 100 nm and exhibit strong light absorption in a wide wavelength range (Figure 5B). The temperature can quickly reach up to about 55°C after 5 min of laser irradiation (1.5 W cm^{-1}), Moreover, the Ta_4C_3-SP nanosheets exhibit good thermal stability even after five heating and cooling cycles (Figure 5B). Without laser irradiation, cell cytotoxicity indicated that Ta_4C_3-SP nanosheets had a negligible effect on the survival of 4T1 cells, even though the concentration was as high as 400 μg ml^{-1}, which indicated its perfect biocompatible property. The photothermal performances depend on laser power density, and this effect was further confirmed by confocal fluorescence imaging after various treatments (Figure 5C). Ta_4C_3-SP nanosheets can rapidly accumulate in the tumor by either intravenous (i.v.) or intratumoral (i.t.) administration in a mouse model, and the temperature of tumor regions quickly increased to 60°C (i.v.) or 68°C (i.t.) from 30°C upon 808-nm laser irradiation for 6 min (Figure 5D). As noted in Figure 5E, Ta_4C_3-SP nanosheets could achieve good photothermal eradication of tumor after irradiation with 808-nm laser. Photographs of 4T1 tumor-bearing mice at 16 days after various treatments are

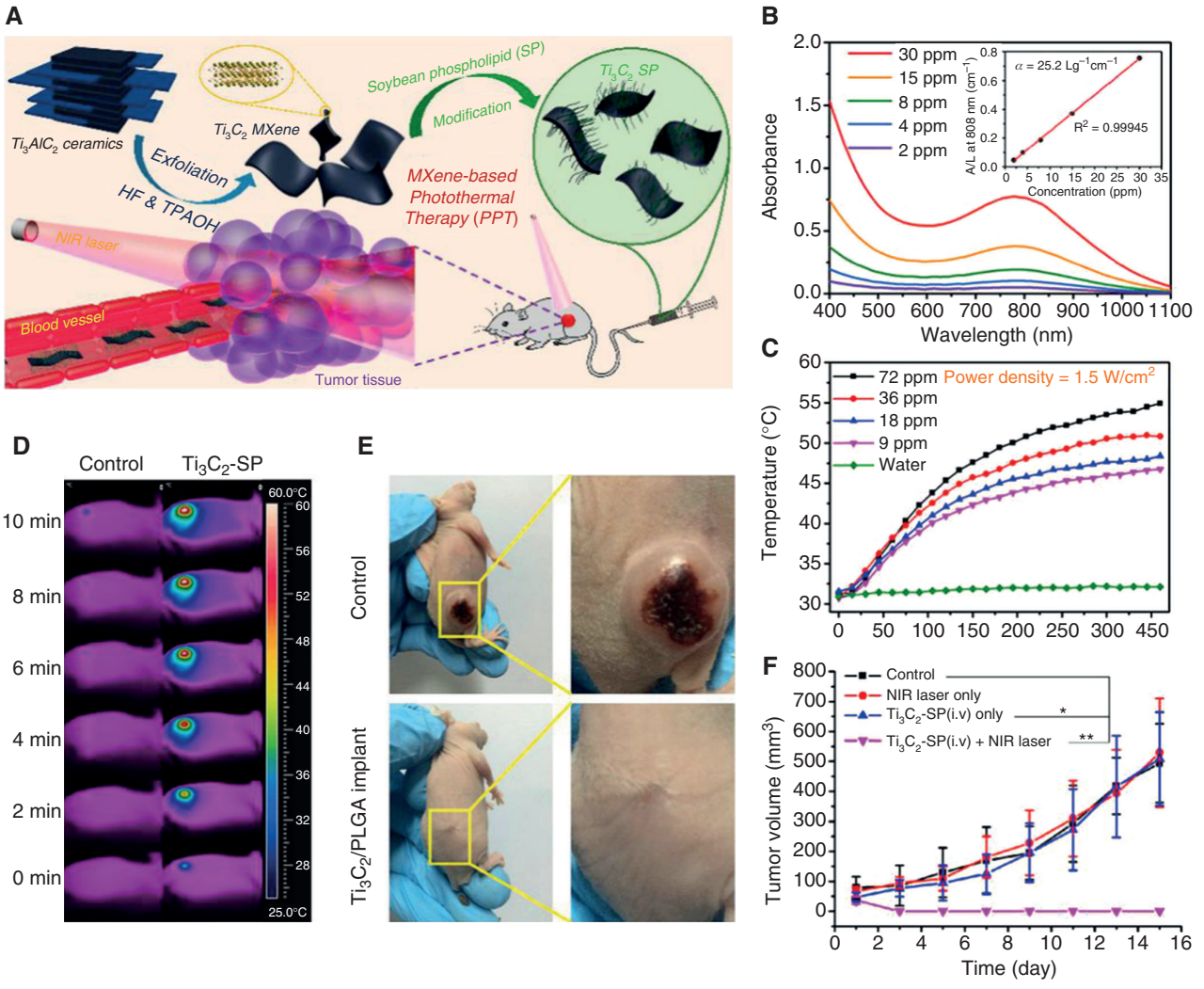

Figure 4: Photothermal profiles of Ti_3C_2-SP MXene nanosheets and its PTT effect in mice model.
(A) Schematic illustration of photothermal ablation of tumor by using Ti_3C_2-SP MXene nanosheets. (B) Absorbance spectra of Ti_3C_2-SP MXene from 400 to 1100 nm. (C) Temperature profile of Ti_3C_2-SP MXene under laser irradiation. (D) Infrared images of tumor-bearing nude mice with or without Ti_3C_2-SP MXene under laser irradiation. (E) Photographs of tumor-bearing mice after PTT. (F) Tumor growth suppression after various treatments.

shown in Figure 5F, which confirmed the good photothermal ablation capacity of Ta_4C_3-SP nanosheets for tumors.

For MXene nanosheets applied in PTT, previous research mainly focused on the first NIR (NIR-I) biowindow (750–1000 nm); however, the second NIR biowindow (NIR-II, 1000–1350 nm) has been rarely explored. Compared with the NIR-I biowindow, the NIR-II biowindow shows a desirably deep tissue penetration depth, reduces tissue scattering, and has few adverse effects due to self-heating in biological environments. Conventional photothermal materials like graphene, MoS_2, and black phosphorus show negligible absorbance in the NIR-II biowindow, which hinders their applications in the NIR-II biowindow. Recently, Lin et al. reported for the first time that Nb_2C nanosheets show both NIR-I and NIR-II absorption with an extraordinarily high photothermal conversion performance [16]. The reported Nb_2C nanosheets exhibited PCE (46.65%) upon 1064-nm laser irradiation and 36.4% upon 808-nm laser irradiation. As a paradigm, the photothermal ablation of tumors in both the NIR-I and NIR-II biowindows was also exploited by taking advantage of Nb_2C-PVP nanosheets as a phototherapeutic agent (Figure 6A). The *in vitro* cytotoxicity indicated that the viability of 4T1 cells decreases with the increase of laser power under both NIR-I and NIR-II irradiation (Figure 6B). In order to compare the tissue penetration depth of NIR-I and NIR-II, light-to-heat conversion was evaluated at various tissue depths under 808- or 1064-nm laser irradiation (Figure 6C). Figure 6D demonstrates that NIR-II laser irradiation can still exhibit effective photothermal conversion after

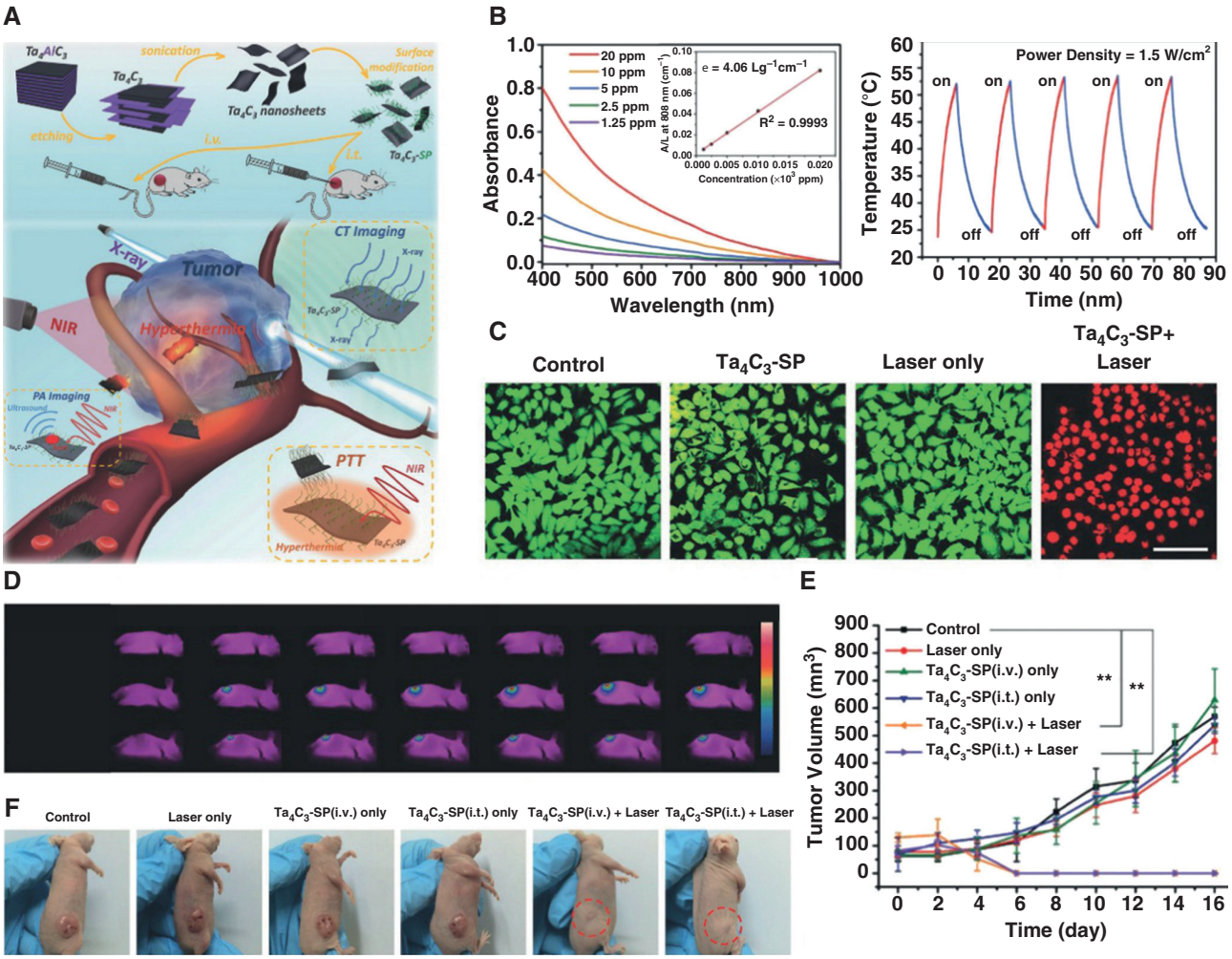

Figure 5: Photothermal therapy effect by Ta_4C_3-SP MXene nanosheets both *in vitro* and *vivo*.
(A) Schematic illustration of Ta_4C_3-SP MXene nanosheets used for PTT. (B) Absorbance spectra and photothermal stability of Ta_4C_3-SP MXene nanosheets under five heating and cooling cycles. (C) *In vitro* photothermal ablation of 4T1 cells after various treatments under 1.5 W cm^{-1} verified by confocal fluorescence imaging (scale bar: 100 μm). (D) Infrared thermal images at the tumor site of 4T1 tumor-bearing mice in groups of control, Ta_4C_3-SP (i.v.) + NIR laser, and Ta_4C_3-SP (i.t.) + NIR laser during laser irradiation at different time intervals. (E) Tumor growth curves after various treatments. (F) Photographs of tumor-bearing mice after PTT.

penetrating a certain depth of *ex vivo* tissue owing to the merits of diminished attenuation in deep tissue. *In vivo* photothermal eradication of tumor xenografts suppressed tumor growth in both the NIR-I and NIR-II biowindows, suggesting the great promise of deep-tissue PTT application (Figure 6E).

4.2 Synergistic therapy

Their inherent planar structure endows MXenes with a large surface area that can serve as a carrier for cargo delivery. Meanwhile, surface engineering integrates versatile therapeutic agents together for multi-functional nanoplatforms to achieve synergistic therapy. MXene-based delivery systems are considered to share the same features as typical delivery systems like inorganic mesoporous carriers, organic nanoplatforms, and 2D planar nanosheets. Owing to the high photothermal conversion of MXenes, synergistic therapy can be achieved by MXene-based PTT and DOX-loaded chemotherapy (Figure 7A). The prepared multi-functional Ti_3C_2 was demonstrated to have high PCE and photothermal stability after undergoing four rounds of heating and cooling cycles [58]. Specifically, the constructed drug delivery nanoplatform showed perfect loading capacity as high as 211.8%, which guaranteed efficient and continuous chemotherapy. More important, this synergistic therapy nanoplatform exhibited pH-responsive and NIR laser-triggered smart on-demand drug release (Figure 7B and C). The *in vitro* synergistic

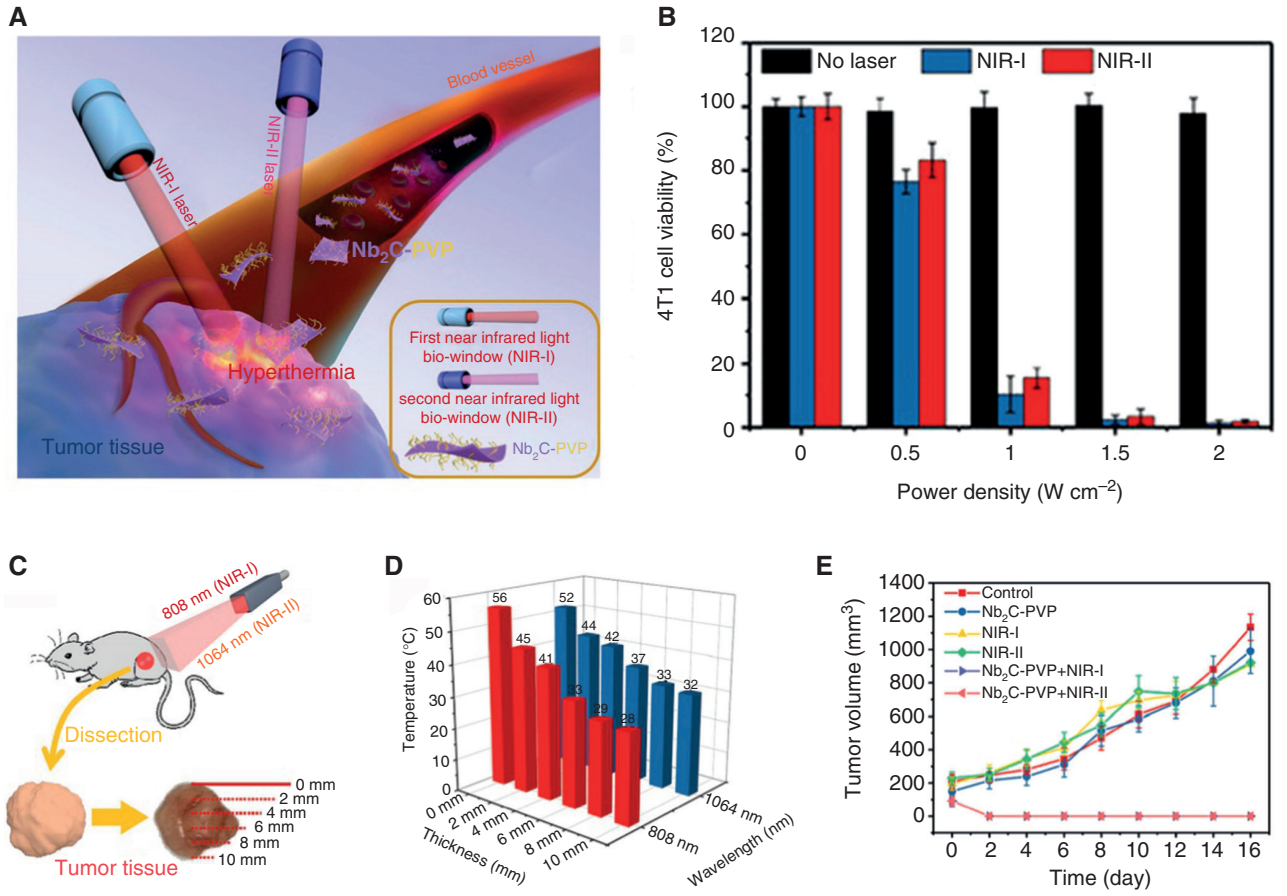

Figure 6: Photothermal therapy for tumor ablation by Nb_2C-PVP Mxene at NIR-II.
(A) Schematic illustration of photothermal tumor ablation in both NIR-I and NIR-II biowindows with Nb_2C-PVP MXene nanosheets. (B) Cytotoxicity evaluation of Nb_2C-PVP MXene nanosheets without and with laser irradiation. (C) NIR-I and NIR-II laser tumor tissue penetration experimental diagram. (D) Photothermal conversion performance of Nb_2C MXene nanosheets in tumor tissues upon NIR-I and NIR-II laser irradiation. (E) Tumor growth curve after various treatments.

therapy performance of Ti_3C_2-based PTT/chemotherapy was further confirmed by confocal laser scanning microscopy (CLSM), indicating that the majority of 4T1 cells were killed after laser treatment (Figure 7D). Further *in vivo* therapeutic treatment evaluation was performed on 4T1 tumor xenograft-bearing mice, and DOX-loaded Ti_3C_2 nanosheets exhibited tumor growth-suppressing property without recurrence.

As an alternative modality of phototherapy, PDT utilizes photosensitizers to transfer its excited-state energy to environmental molecular oxygen species for ROS generation under light irradiation. Subsequently, tumor cells are killed by imposing oxidized pressure on cellular substances. PDT has several merits for oncologic intervention, such as minimal invasiveness and few adverse effects. MXenes as a photodynamic agent for cancer therapy have been reported to act through ROS generation, while the generation mechanism still needs to be explored. Integrating phototherapy like PDT or PTT with chemotherapy could provide synergistic therapy for efficient tumor ablation. Dong et al. reported on Ti_3C_2 nanosheet-based synergistic therapeutics combining PTT/PDT/chemotherapy by multi-layer construction with DOX as the chemotherapy drug (Figure 7E) [17]. This new synergistic nanoplatform showed a considerably high drug-loading efficiency (84.2%). Meanwhile, Ti_3C_2-DOX enables effective local heat generation under NIR laser irradiation (up to 50°C) and drug release in acidic environment is accelerated by local heating (Figure 7F). ROS generation was measured using the fluorescence intensity of the ROS probe (dichloro-dihydro-fluorescein diacetate) after NIR laser irradiation. Further *in vivo* study indicated the favorable specific tumor accumulation and ROS generation after 808-nm laser irradiation (Figure 7G). Animal experiments showed efficient tumor ablation after administration of a dose of 2 mg kg^{-1} of Ti_3C_2-DOX nanosheet in a mouse model, demonstrating an effective synergistic therapeutic outcome (Figure 7H).

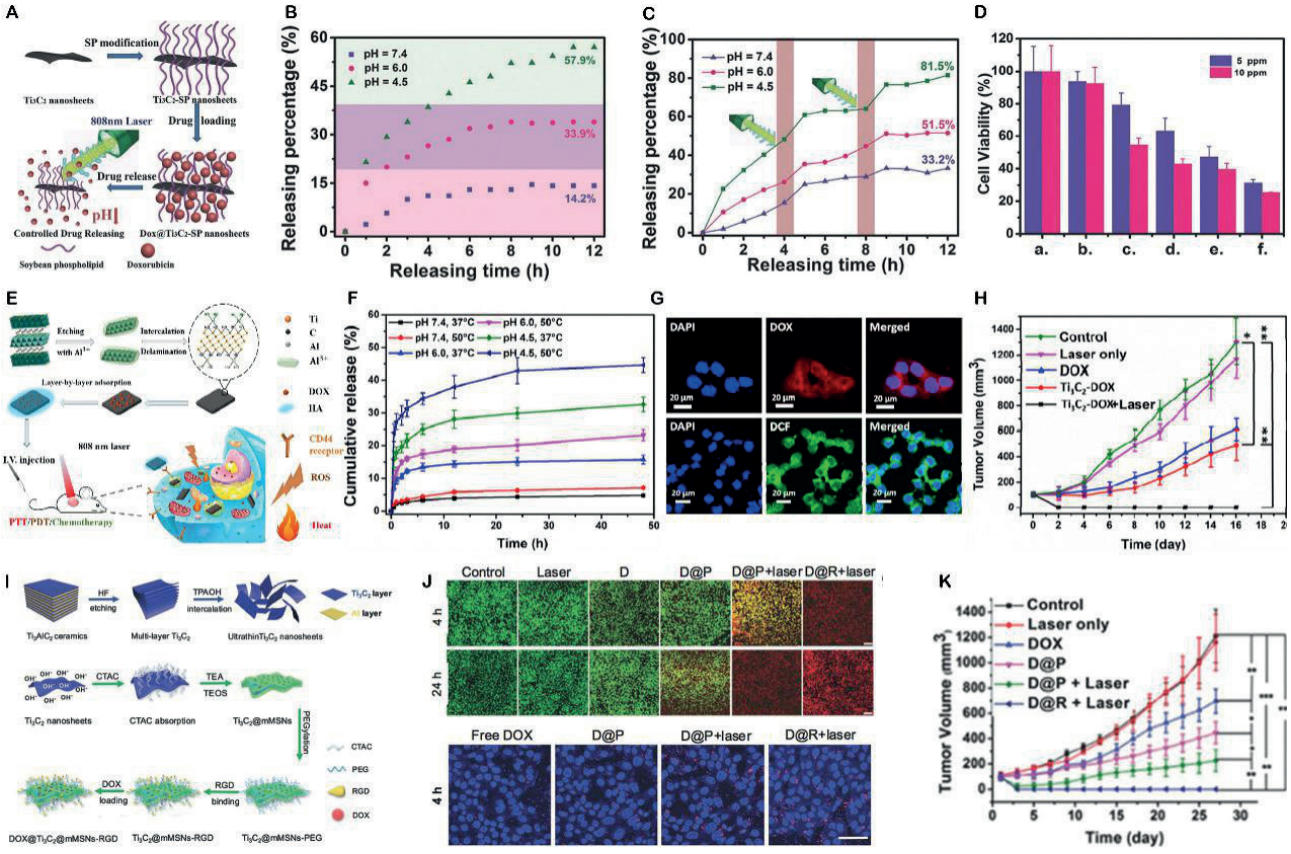

Figure 7: Synergistic and targeting therapy by various MXene system.
(A) Schematic illustration of surface modification of Ti_3C_2 nanosheets and stimuli-responsive drug releasing by pH decrease or laser irradiation. (B) pH-responsive DOX-releasing profiles. (C) Laser-induced DOX-releasing performance under different pH values (7.4, 6.0, and 4.5) (D) Cytotoxicity of 4T1 cells after various concentrations of DOX@Ti_3C_2-SP nanosheet treatments. (E) Schematic illustration of synergetic therapy platform integrated PTT/PDT/chemotherapy on Ti_3C_2 nanosheets. (F) Drug-releasing profiles under 808-nm laser irradiation at various pH values (4.5, 6.0, and 7.4). (G) Fluorescence images of HCT-116 cells after DOX@Ti_3C_2-SP treatment and ROS generation imaging after 808-nm laser irradiation (0.8 W cm^{-2}, 10 min). (H) Tumor suppression effect after various treatments. (I) Schematic illustration of surface nanopore engineering Ti_3C_2 MXene nanosheets, DOX loading, and RGD modification process. (J) Fluorescence imaging of HCC cells stained by calcein AM (green) and propidium iodide (red) after 4- and 24-h incubation with various therapy agents. (K) Tumor growth curves after different treatments.

4.3 Targeting therapy

Efficient phototherapy requires enhanced accumulation of therapeutic agents to the tumor site or pathological region. The majority of therapeutic agents are delivered to the tumor site via EPR, also known as passive targeting. Compared with passive targeting, the recently developed active targeting is an alternative strategy for high accumulation of drug carriers or therapeutic agents to target sites. Specially, by surface modification of hyaluronic acid (HA) on Ti_3C_2, a tumor-specific recognition photothermal agent can be achieved. Benefiting from the specific recognition between HA and $CD44^+$ that are overexpressed on the tumor cells, the HA-modified Ti_3C_2-DOX can be targeted and accumulated on the tumor cells (Figure 7E). The anticancer agent has been evidenced to selectively accumulate in the tumor site in both *in vitro* and *in vivo* experiments, which lay the foundation for an efficient PTT [17].

Surface nanopore engineering of 2D MXene Ti_3C_2 nanosheets with a nanothin mesoporous nanostructure for drug loading and RGD-targeted functionalization for tumor-specific targeting have been recently reported (referred to as Ti_3C_2@mMSN-RGD) [43]. The schematic illustration is shown in Figure 7I. The multi-therapeutic nanoplatform demonstrated outstanding photothermal performance. CLSM images are shown in Figure 7G. Ti_3C_2@mMSNs functionalized with RGD have better cell suppression effect compared to those without RGD modification. One explanation for the different growth suppression of HCC cells is that Ti_3C_2@mMSN-RGD exhibited evident superior active-targeting capability owing to the strongly anchored force between the RGD peptides and the ligands

expressed on the hepatocellular carcinoma (HCC) cell membranes, which facilitated a large number of therapeutic agents targeting the HCC cells via endocytosis. The *in vivo* therapeutic effect was systematically evaluated, and the results indicated that the high active-targeting outcome of Ti_3C_2@mMSN-RGD in tumors can be ascribed to RGD recognition and synergetic ablation of tumor (chemotherapy and PTT) without future tumor recurrence (Figure 7K). In the PTT process, MXenes have been well developed as PAI agents for monitoring the treatment progress [41]. Due to their superior features of 3D imaging, deep penetration, and high spatial resolution, the MXene-based PAI enables realizing the imaging-guided theranostics. Noteworthy, other bioimaging modalities like fluorescent cell imaging and multi-mode bioimaging [MRI/computed tomography (CT)] have been successfully established and have shown potential in clinical diagnostic imaging [14, 54, 57].

5 Biosafety evaluations

The biological application of MXenes has increasingly drawn attention owing to their inherent characteristics such as 2D morphology or structure, facile surface engineering, versatile functionality, and physicochemical stability. Recent studies have demonstrated their potential practical translation; however, there are still many challenges to be addressed before their clinical translation, such as biosafety and long-term cytotoxicity. Thus, systematic investigations on biosafety and long-term cytotoxicity are critical for further biomedical applications. Studies have demonstrated their low cytotoxicity and biocompatibility by culturing with cells. For example, the reported PTT agent Ti_3C_2-SP nanosheets show negligible cytotoxicity with a high 4T1 cell survival after 2 days of co-incubation even at a high concentration of 600 ppm (Figure 8A) [59]. The same effect can be found in MnO_x/Ti_3C_2-SP nanosheets using the same evaluation method, and the result also indicated high cell viability (Figure 8B) [10]. Recent work has investigated the metabolism and excretion of Ti_3C_2 MXene nanosheet surface coated with SP in the nude mouse model. The results showed that Ti_3C_2-SP can be gradually excreted out of the body via urine and feces with amounts of 18.7% and 10.35%, respectively, at 2 days after injection, which indicated the biodegradable property. The potential biosafety and biocompatibility of another surface-modified MXene, Nb_2C nanosheets, were also evaluated against the 4T1 and U87 cell lines (Figure 8C). *In vivo* biosafety examination was carried out by administering 20 mg kg^{-1} of Nb_2C-PVP nanosheets in a mouse model. Negligible abnormal behavior and body weight change were observed during the treatment period. Tissue slices and staining of major organs exhibited no obvious acute, chronic pathological toxicity and adverse effects, which was further confirmed by measuring the hematological indices and biochemistry parameters in the blood tests (Figure 8D) [16].

Besides those achievements, ecotoxicological assessments were conducted using a zebrafish embryo model. A concentration-dependent manner of uptake and no obvious teratogenic effects were observed in zebrafish embryos at 100 mg ml^{-1} of Ti_3C_2 under open conditions (Figure 8E, i). Additionally, there was a negligible toxicity effect confirmed by locomotion and neurotoxicity assays, which showed no harmful effect on neuromuscular activities (50 μg l^{-1}) (Figure 8E, ii–iii). $Ti_3C_2T_x$ MXene was suggested to be classifiable into the "practically non-toxic" group in terms of the regulations of the Acute Toxicity Rating Scale by the Fish and Wildlife Service [60]. To date, although the biocompatibility and long-term toxicity have been studied *in vitro* and *vivo* in lower animal models like zebra fish or mice, the long-term toxicity, immunogenicity, pharmacokinetics, and biodistribution of MXenes also need to be further investigated in higher mammals like dogs, rabbits, and monkeys.

6 Conclusions and perspectives

Because of the unique features of MXenes, researchers have made great efforts to develop approaches for their synthesis, surface functionalization, and photothermal application in the biomedical field. The photothermal applications of MXenes are listed in Table 1, with the synthesis methods, surface modification profiles, optical properties, and PCE. Compared with traditional photothermal agents like graphene, MoS_2, and organic materials, the overall photothermal performance of MXenes seems better. Although the reported MXenes have demonstrated promising results in PTT, there are still challenges that need to be addressed before the clinical translation of these materials.

In terms of synthesis methods, theoretical simulations have predicted a large number of MXenes, whereas the recent experimentally demonstrated species are much fewer. Specifically, W_2C and Zr_2C could be synthesized by etching their corresponding MAX phase or non-MAX phase precursors, and the photothermal property is worthy of future investigation. In addition, the theoretically indicated

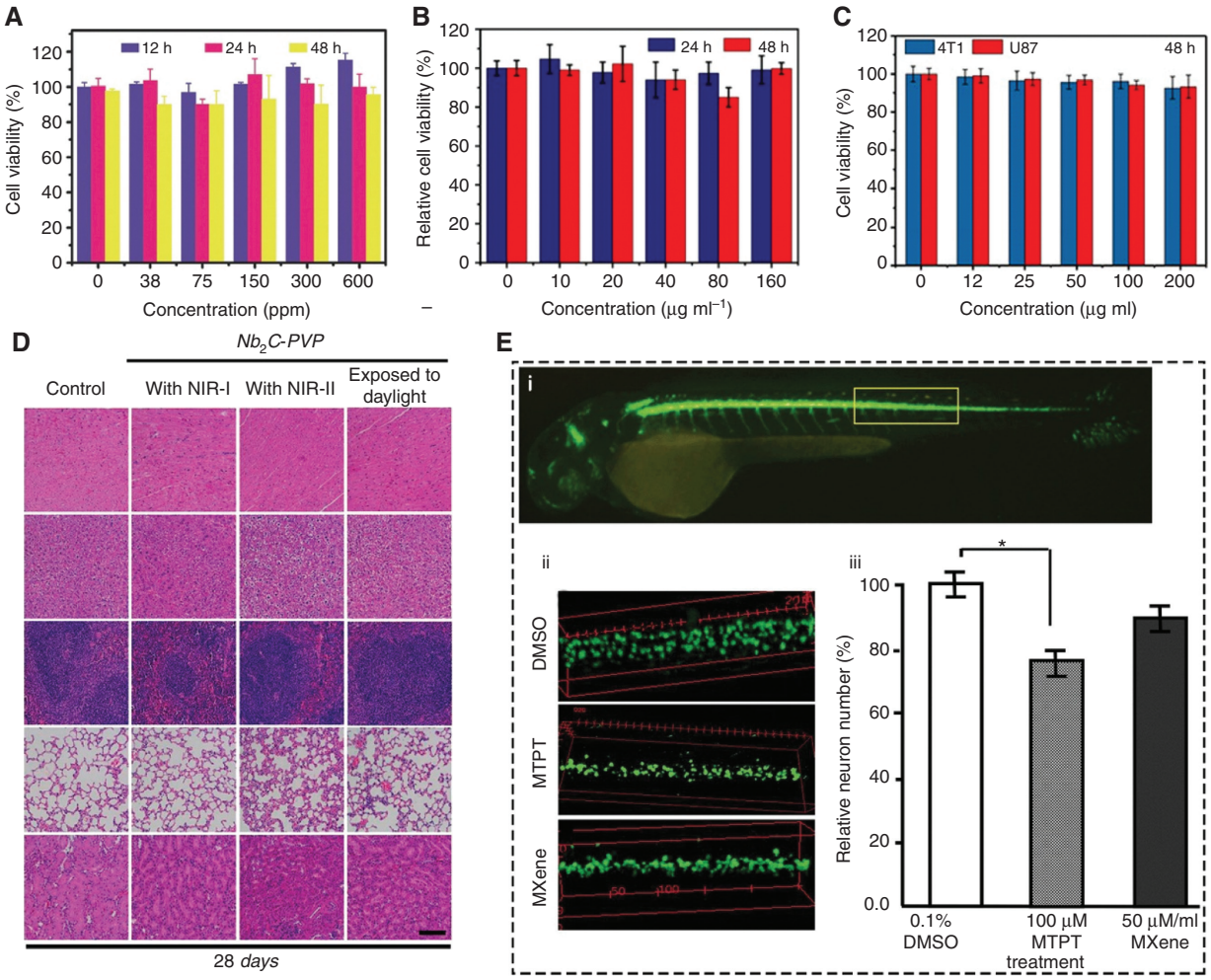

Figure 8: Biocompatibility study of the various concentrations of MXenes on the 4T1 cell line or U87 cells. (A) Ti_3C_2-SP nanosheets. (B) MnO_x/Ti_3C_2-SP nanosheets. (C) Nb_2C-PVP nanosheets. (D) Hematoxylin and eosin staining for major organs after Nb_2C-PVP nanosheet treatment at 28 days after injection under NIR-I, NIR-II, and daylight (scale bars: 100 μm). (E) i, fluorescence imaging of an entire embryo; ii, confocal pictures of the spinal cord adjacent to the somite 14–17 territory after treatments with DMSO, 1-methyl-4-phenyl-1,2,3,6-tetrahydropyridine hydrochloride (MTPT), and MXene; iii, average of the relative neuronal number of 14 treated embryos *$p < 0.05$.

V_2N, Ti_2N, and V_4C_3 are promising for energy storage applications or in the catalysis field. Thus, more efforts should be devoted to exploring novel MXenes with unique properties, like multi-component metal-doped MXenes, which are expected to possess higher PCE. Meanwhile, the most reported MXenes possess intense light absorption at NIR-I. MXenes at NIR-II absorption have rarely been realized except for the Nb_2C nanosheets. Rationally designing their compositions to explore their unique properties in the NIR-II biowindow will significantly broaden the PTT applications with desirable tissue penetration depth.

Apparently, the surface terminations of MXenes are strongly related to their properties. It is highly expected that surface modification will provide diverse multi-functional nanoplatforms for future biological applications. However, the MXene surface modifications are limited to non-covalent interactions on the surface of MXenes, like PEG, PVP, and SP. Surface modification endows the MXenes not only biocompatibility but also multi-functional property, like targeting ligands for preferential accumulation in the tumor site. However, the developed coating agents still do not satisfy the biomedical demand and still need to be thoroughly explored.

Last but not least, the multi-function-integrated MXene nanoplatform should be further designed and developed for meeting the diversified demands for biological applications. Multifunctional MXenes that integrate magnetic, light-harvesting, and photothermal conversion properties can provide new horizons for advanced PTT treatment of cancer, by which multimodality theranostics can be achieved to offer more powerful tools in treating and imaging biomedical issues.

Table 1: Application of MXenes in PTT.

Materials	Preparation method	Surface modification	Absorption range (nm)	Application	Laser wavelength (nm)	PCE	Reference
Ti_3C_2-DOX	HF etching	SP	400–900	PTT/chemotherapy for tumor	808	NA	[50]
Ta_4C_3-MnO_x	HF etching	SP	400–850	PTT/MRI/CT for tumor	808	34.9%	[34]
Ti_3C_2@mMSNs	HF etching	PEG/RGD	400–1200	Synergetic tumor therapy	808	23.2%	[36]
Nb_2C	HF etching	PVP	350–1200	PTT for tumor	808, 1064	36.4% (808 nm), 45.65% (1064 nm)	[16]
MnO_x/Ti_3C_2	HF etching	SP	400–1000	PTT/MRI for tumor	808	22.9%	[10]
Ta_4C_3-Fe_3O_4	HF etching	SP	300–1000	PTT/MRI for tumor	808	32.5%	[11]
Ti_3C_2-DOX	HF etching	HA	400–1100	PTT/PDT/chemotherapy for tumor	808	58.3%	[17]
PLGA/Ti_3C_2	HF etching	SP	400–1100	PTT for tumor	808	30.6%	[48]
GdW_{10}@Ti_3C_2	HF etching	PEG/BSA	200–1000	PTT/MRI/CT for tumor	808	44.9%	[32]
Ta_4C_3	HF etching	SP	400–1000	PTT for tumor	808	44.7%	[49]
Ti_3C_2 QDs	TBAOH delamination	Al oxyanions	200–1100	PTT for tumor	808	52.2%	[21]
Ti_3C_2	TMAOH delamination	PEG	400–1300	PTT for tumor	808	NA	[24]
Ti_3C_2	HF etching	-OH, -O, -F	300–1300	Solar steam generation	Solar light	~100%	[46]
Ti_3C_2 membrane	HF etching	-OH, -O, -F	250–2500	Solar steam generation	Solar light	NA	[7]
$Ti_3C_2T_x$/PVDF film	HF etching	-OH, -O, -F	NA	Antibacterial	NA	NA	[52]
Ti_3C_2	HF etching	-OH, -O, -F	NA	Antibacterial	NA	NA	[53]

Meanwhile, the microenvironment-responsive MXene-based nanoplatform, mainly including pH response, temperature response, and functional small biological-molecular response, should also be developed for the intelligent delivery of drugs and probes, in which the efficient treatment and diagnosis with fewer adverse effects can be realized. As evidenced by their good photothermal conversion performance, the new application of MXenes in other fields should be further explored, such as pollutant cleaning, seawater evaporation, and bioactive regulation. Overall, MXene-based materials will play significant roles in photothermal applications in the future. More efforts should be devoted to MXene-based photothermal applications as well as diagnostic imaging, biosensing, antimicrobial evaluation, and biosafety evaluation.

Acknowledgments: The work described in this article was supported by a grant from the University Grants Committee/Research Grants Council of the Hong Kong Special Administrative Region, China (project no. JLFS/P-101/18), Hong Kong Innovation and Technology Commission (project no. ITS/219/19), and ARG-CityU Applied Research Grant (project nos. 9667160, 9667179).

Conflict of interest: The authors declare no conflict of interest.

References

[1] Naguib M, Kurtoglu M, Presser V, et al. Two-dimensional nanocrystals produced by exfoliation of Ti_3AlC_2. Adv Mater 2011;23:4248–53.
[2] Anasori B, Lukatskaya MR, Gogotsi Y. 2D metal carbides and nitrides (MXenes) for energy storage. Nat Rev Mater 2017;2:16098.
[3] Enyashin AN, Ivanovskii AL. Structural and electronic properties and stability of MXenes Ti_2C and Ti_3C_2 functionalized by methoxy groups. J Phys Chem C 2013;117:13637–43.
[4] Gogotsi Y, Anasori B. The rise of MXenes. ACS Nano 2019;13:8491–4.
[5] Ghidiu M, Lukatskaya MR, Zhao MQ, Gogotsi Y, Barsoum MW. Conductive two-dimensional titanium carbide 'clay' with high volumetric capacitance. Nature 2014;516:78.
[6] Peng J, Chen X, Ong WJ, Zhao X, Li N. Surface and heterointerface engineering of 2D MXenes and their nanocomposites: insights into electro- and photocatalysis. Chem 2019;5:18–50.
[7] Zhao J, Yang Y, Yang C, et al. A hydrophobic surface enabled salt-blocking 2D Ti_3C_2 MXene membrane for efficient and stable solar desalination. J Mater Chem A 2018;6:16196–204.
[8] Liu H, Duan C, Yang C, Shen W, Wang F, Zhu Z. A novel nitrite biosensor based on the direct electrochemistry of hemoglobin immobilized on MXene-Ti_3C_2. Sensors Actuat B Chem 2015;218:60–6.
[9] Mayerberger EA, Street RM, McDaniel RM, Barsoum MW, Schauer CL. Antibacterial properties of electrospun Ti_3C_2Tz (MXene)/chitosan nanofibers. RSC Adv 2018;8:35386–94.
[10] Dai C, Lin H, Xu G, Liu Z, Wu R, Chen Y. Biocompatible 2D titanium carbide (MXenes) composite nanosheets for pH-responsive MRI-guided tumor hyperthermia. Chem Mater 2017;29:8637–52.

[11] Liu Z, Lin H, Zhao M, et al. 2D superparamagnetic tantalum carbide composite MXenes for efficient breast-cancer theranostics. Theranostics 2018;8:1648–64.
[12] Naguib M, Mochalin VN, Barsoum MW, Gogotsi Y. 25th anniversary article: MXenes: a new family of two-dimensional materials. Adv Mater 2014;26:992–1005.
[13] Lin H, Chen Y, Shi J. Insights into 2D MXenes for versatile biomedical applications: Current advances and challenges ahead. Adv Sci 2018;5:1800518.
[14] Xue Q, Zhang H, Zhu M, et al. Photoluminescent Ti_3C_2 MXene quantum dots for multicolor cellular imaging. Adv Mater 2017;29:1604847.
[15] Wang Z, Xuan J, Zhao Z, Li Q, Geng F. Versatile cutting method for producing fluorescent ultra-small MXene sheets. ACS Nano 2017;11:11559–65.
[16] Lin H, Gao S, Dai C, Chen Y, Shi J. A two-dimensional biodegradable niobium carbide (MXene) for photothermal tumor eradication in NIR-I and NIR-II biowindows. J Am Chem Soc 2017;139:16235–47.
[17] Liu G, Zou J, Tang Q, et al. Surface modified Ti_3C_2 MXene nanosheets for tumor targeting photothermal/photodynamic/chemo synergistic therapy. ACS App Mater Inter 2017;9:40077–86.
[18] Tao W, Kong N, Ji X, et al. Emerging two-dimensional monoelemental materials (Xenes) for biomedical applications. Chem Soc Rev 2019;48:2891–912.
[19] Ji X, Kong Y, Ouyang J, et al. Synthesis of ultrathin biotite nanosheets as an intelligent theranostic platform for combination cancer therapy. Adv Sci 2019;6:1901211.
[20] Ouyang J, Feng C, Ji X, et al. 2D monoelemental germanene quantum dots: synthesis as robust photothermal agents for photonic cancer nanomedicine. Angew Chem Int Ed 2019;131:13539–44.
[21] Tao W, Zhu X, Yu X, et al. Black phosphorus nanosheets as a robust delivery platform for cancer theranostics. Adv Mater 2017;29:1603276.
[22] Tao W, Ji X, Zhu X, et al. Two-dimensional antimonene-based photonic nanomedicine for cancer theranostics. Adv Mater 2018;30:1802061.
[23] Tao W, Ji X, Xu X, et al. Antimonene quantum dots: synthesis and application as near-infrared photothermal agents for effective cancer therapy. Angew Chem Int Ed 2017;56:11896–900.
[24] Li S, Chen Y, Liu H, et al. Graphdiyne materials as nanotransducer for in vivo photoacoustic imaging and photothermal therapy of tumor. Chem Mater 2017;29:6087–94.
[25] Naguib M, Mashtalir O, Carle J, et al. Two-dimensional transition metal carbides. ACS Nano 2012;6:1322–31.
[26] Wang H, Li H, Huang Y, Xiong M, Wang F, Li C. A label-free electrochemical biosensor for highly sensitive detection of gliotoxin based on DNA nanostructure/MXene nanocomplexes. Biosens Bioelectron 2019;142:111531.
[27] Mashtalir O, Naguib M, Mochalin VN, et al. Intercalation and delamination of layered carbides and carbonitrides. Nat Commun 2013;4:1716.
[28] Yu X, Cai X, Cui H, Lee SW, Yu XF, Liu B. Fluorine-free preparation of titanium carbide MXene quantum dots with high near-infrared photothermal performances for cancer therapy. Nanoscale 2017;9:17859–64.
[29] Lee E, Vahid Mohammadi A, Prorok BC, Yoon YS, Beidaghi M, Kim DJ. Room temperature gas sensing of two-dimensional titanium carbide (MXene). ACS App Mater Inter 2017;9:37184–90.
[30] Ghidiu M, Halim J, Kota S, Bish D, Gogotsi Y, Barsoum MW. Ion-exchange and cation solvation reactions in Ti_3C_2 MXene. Chem Mater 2016;28:3507–14.
[31] Xuan J, Wang Z, Chen Y, et al. Organic-base-driven intercalation and delamination for the production of functionalized titanium carbide nanosheets with superior photothermal therapeutic performance. Angew Chem Inter Ed 2016;55:14569–74.
[32] Yang S, Zhang P, Wang F, et al. Fluoride-free synthesis of two-dimensional titanium carbide (MXene) using a binary aqueous system. Angew Chem Inter Ed 2018;130:15717–21.
[33] Pang SY, Wong YT, Yuan S, et al. Universal strategy for HF-free facile and rapid synthesis of two-dimensional MXenes as multifunctional energy materials. J Am Chem Soc 2019;141:9610–6.
[34] Ito Y, Tanabe Y, Han J, Fujita T, Tanigaki K, Chen M. Multifunctional porous graphene for high-efficiency steam generation by heat localization. Adv Mater 2015;27:4302–7.
[35] Xing W, Tu W, Han Z, Hu Y, Meng Q, Chen G. Template-induced high-crystalline g-C_3N_4 nanosheets for enhanced photocatalytic H_2 evolution. ACS Energy Lett 2018;3:514–9.
[36] Yang G, Gu Y, Yan P, et al. Chemical vapor deposition growth of vertical MoS_2 nanosheets on p-GaN nanorods for photodetector application. ACS App Mater Inter 2019;11:8453–60.
[37] Xu C, Wang L, Liu Z, et al. Large-area high-quality 2D ultrathin Mo_2C superconducting crystals. Nat Mater 2015;14:1135.
[38] Soleymaniha M, Shahbazi MA, Rafieerad AR, Maleki A, Amiri A. Promoting role of MXene nanosheets in biomedical sciences: therapeutic and biosensing innovations. Adv Healthc Mater 2019;8:1801137.
[39] Zong L, Wu H, Lin H, Chen Y. A polyoxometalate-functionalized two-dimensional titanium carbide composite MXene for effective cancer theranostics. Nano Res 2018;11:4149–68.
[40] Liu Z, Zhao M, Lin H, et al. 2D magnetic titanium carbide MXene for cancer theranostics. J Mater Chem B 2018;6:3541–8.
[41] Dai C, Chen Y, Jing X, et al. Two-dimensional tantalum carbide (MXenes) composite nanosheets for multiple imaging-guided photothermal tumor ablation. ACS Nano 2017;11:12696–712.
[42] Xing C, Chen S, Liang X, et al. Two-dimensional MXene (Ti_3C_2)-integrated cellulose hydrogels: Toward smart three-dimensional network nanoplatforms exhibiting light-induced swelling and bimodal photothermal/chemotherapy anticancer activity. ACS Appl Mater Inter 2018;10:27631–43.
[43] Li Z, Zhang H, Han J, Chen Y, Lin H, Yang T. Surface nanopore engineering of 2D MXenes for targeted and synergistic multitherapies of hepatocellular carcinoma. Adv Mater 2018;30:1706981.
[44] Berdiyorov GR. Optical properties of functionalized $Ti_3C_2T_2$ (T = F, O, OH) MXene: first-principles calculations. AIP Adv 2016;6:055105.
[45] Zhang H, Yang G, Zuo X, Tang H, Yang Q, Li G. Computational studies on the structural electronic and optical properties of graphene-like MXenes (M_2CT_2M = TiZrHfT = O, F, OH) and their potential applications as visible-light driven photocatalysts. J Mater Chem A 2016;4:12913–20.
[46] Sarycheva A, Makaryan T, Maleski K, et al. Two-dimensional titanium carbide (MXene) as surface-enhanced Raman scattering substrate. J Phys Chem C 2017;121:19983–88.
[47] Hu M, Li Z, Hu T, Zhu S, Zhang C, Wang X. High-capacitance mechanism for $Ti_3C_2T_x$ MXene by *in situ* electrochemical Raman spectroscopy investigation. ACS Nano 2016;10:11344–50.

[48] Lipatov A, Alhabeb M, Lukatskaya MR, Boson A, Gogotsi Y, Sinitskii A. Effect of synthesis on quality electronic properties and environmental stability of individual monolayer Ti_3C_2 MXene flakes. Adv Electron Mater 2016;2:1600255.
[49] Feng L, Zha XH, Luo K, et al. Structures and mechanical and electronic properties of the Ti_2CO_2 MXene incorporated with neighboring elements (Sc, V, B and N). J Electron Mater 2017;46:2460–6.
[50] Xiao B, Li YC, Yu XF, Cheng JB. MXenes: reusable materials for NH_3 sensor or capturer by controlling the charge injection. Sensors Actuat B Chem 2016;235:103–9.
[51] Zha XH, Luo K, Li Q, et al. Role of the surface effect on the structural electronic and mechanical properties of the carbide MXenes. Europhys Lett 2015;111:26007.
[52] Yang J, Luo X, Zhou X, et al. Tuning magnetic properties of $Cr_2M_2C_3T_2$ (M = Ti and V) using extensile strain. Comp Mater Sci 2017;139:313–9.
[53] Li R, Zhang L, Shi L, Wang P. MXene Ti_3C_2: an effective 2D light-to-heat conversion material. ACS Nano 2017;11:3752–9.
[54] Lin H, Wang X, Yu L, Chen Y, Shi J. Two-dimensional ultrathin MXene ceramic nanosheets for photothermal conversion. Nano Lett 2017;17:384–91.
[55] Huang P, Rong P, Lin J, et al. Triphase interface synthesis of plasmonic gold bellflowers as near-infrared light mediated acoustic and thermal theranostics. J Am Chem Soc 2014;136:8307–13.
[56] Lin H, Wang Y, Gao S, Chen Y, Shi J. Theranostic 2D tantalum carbide (MXene). Adv Mater 2018;30:1703284.
[57] Han X, Huang J, Lin H, Wang Z, Li P, Chen Y. 2D ultrathin MXene-based drug-delivery nanoplatform for synergistic photothermal ablation and chemotherapy of cancer. Adv Healthc Mater 2018;7:1701394.
[58] Nasrallah GK, Al-Asmakh M, Rasool K, Mahmoud KA. Ecotoxicological assessment of $Ti_3C_2T_x$ (MXene) using a zebrafish embryo model. Environ Sci Nano 2018;5:1002–11.
[59] Rasool K, Helal M, Ali A, Ren CE, Gogotsi Y, Mahmoud KA. Antibacterial activity of $Ti_3C_2T_x$ MXene. ACS Nano 2016;10:3674–84.
[60] Rasool K, Mahmoud KA, Johnson DJ, Helal M, Berdiyorov GR, Gogotsi Y. Efficient antibacterial membrane based on two-dimensional $Ti_3C_2T_x$ (MXene) nanosheets. Sci Rep 2017;7:1598.